Parasites & Vectors

RESEARCH

Open Access

Honokiol induces apoptosis-like death in *Cryptocaryon irritans* Tomont

Zi-Chen Zhao[1,2], Man-Yi Jiang[1], Ji-Hui Huang[1,4], Chuan Lin[3], Wei-Liang Guo[1*], Zhi-Hong Zhong[1], Qing-Qin Huang[1], Shao-Long Liu[1], Heng-Wei Deng[1] and Yong-Can Zhou[1*]

Abstract

Background *Cryptocaryon irritans*, a common parasite in tropical and subtropical marine teleost fish, has caused serious harm to the marine aquaculture industry. Honokiol was proven to induce *C. irritans* tomont cytoplasm shrinkage and death in our previous study, but the mechanism by which it works remains unknown.

Methods In this study, the changes of apoptotic morphology and apoptotic ratio were detected by microscopic observation and AnnexinV-FITC/PI staining. The effects of honokiol on intracellular calcium ($[Ca^{2+}]_i$) concentration, mitochondrial membrane potential ($\Delta\Psi m$), reactive oxygen species (ROS), quantity of DNA fragmentations (QDF) and caspase activities were detected by Fluo-3 staining, JC-1 staining, DCFH-DA staining, Tunel method and caspase activity assay kit. The effects of honokiol on mRNA expression levels of 61 apoptosis-related genes in tomonts of *C. irritans* were detected by real-time PCR.

Results The results of the study on the effects of honokiol concentration on *C. irritans* tomont apoptosis-like death showed that the highest levels of prophase apoptosis-like death rate (PADR), $[Ca^{2+}]_i$ concentration, ROS, the activities of caspase-3/9 and the lowest necrosis ratio (NER) were obtained at a concentration of 1 μg/ml, which was considered the most suitable for inducing *C. irritans* tomont apoptosis-like death. When *C. irritans* tomonts were treated with 1 μg/ml honokiol, the $[Ca^{2+}]_i$ concentration began to increase significantly at 1 h. Following this, the ROS, QDF and activities of caspase-3/9 began to increase significantly, and the $\Delta\Psi m$ began to decrease significantly at 2 h; the highest PADR was obtained at 4 h. The mRNA expression of 14 genes was significantly upregulated during honokiol treatment. Of these genes, *itpr2*, *capn1*, *mc*, *actg1*, *actb*, *parp2*, *traf2* and *fos* were enriched in the pathway related to apoptosis induced by endoplasmic reticulum (ER) stress.

Conclusions This article shows that honokiol can induce *C. irritans* tomont apoptosis-like death. These results suggest that honokiol may disrupt $[Ca^{2+}]_i$ homeostasis in ER and then induce *C. irritans* tomont apoptosis-like death by caspase cascade or mitochondrial pathway, which might represent a novel therapeutic intervention for *C. irritans* infection.

Keywords *Cryptocaryon irritans*, Honokiol, Apoptosis-like death, Endoplasmic reticulum stress

*Correspondence:
Wei-Liang Guo
guowl07@hainanu.edu.cn
Yong-Can Zhou
zychnu@hainanu.edu.cn
Full list of author information is available at the end of the article

Background

Cryptocaryon irritans, a common protozoan parasite of marine teleost fish, causes "white spot" disease [1]. This disease is mainly prevalent in tropical and subtropical sea areas [2–4]. Its life cycle includes four stages: trophont, protomont, tomont, and theront [5]. Tomont is the longest-lasting, free-living stage of *C. irritans*. Tomonts have strong resistance to drugs and harsh environments because of their hard cysts. Tomonts can still produce infectious theronts after being preserved at 12 °C for 3 months [5]. It is difficult to completely remove *C. irritans* tomonts in an open mariculture environment, which makes the prevention and control of white spot disease very difficult. It is a good strategy to prevent and treat parasites by inducing their spontaneous death; this has the advantages of low probability of drug resistance and host inflammation. It is well known that apoptosis is a highly regulated process of cell death [6]. In recent years, apoptosis has provided a new treatment for many diseases, such as inflammation, cancer, leishmaniasis, malaria, and toxoplasmosis [7–14]. The apoptosis-like death pathway has also been found in many protozoa, such as Leishmania, *Plasmodium falciparum*, *Tetrahymena thermophila*, *Trypanosoma cruzi*, *Blastocystis hominis*, *Toxoplasma gondii*, and *Ichthyophthirius multifiliis* [12–21], providing a new way to treat parasitic diseases. Many apoptosis-related genes of *C. irritans* have been found via transcriptome analysis [22–26], which indicates that *C. irritans* might have an apoptosis-like death pathway. Honokiol, one of the main active components of *Magnolia officinalis*, has been reported to induce apoptosis of cancer cells and *Candida albicans* via the endoplasmic reticulum (ER) stress pathway [27–30]. Our previous studies demonstrated that honokiol significantly inhibited the proliferation and hatching of *C. irritans* tomonts. The resulting *C. irritans* tomont cytoplasm obviously shrank without cytoplasm or cell membrane damage [31], indicating that honokiol might induce *C. irritans* tomont apoptosis-like death. However, further experiments are needed to confirm this speculation, and the mechanism remains to be uncovered.

In this article, Annexin V-FITC/PI staining was used to determine whether honokiol induces *C. irritans* tomont apoptosis-like death. The effects of honokiol at various treating concentrations and times on the morphologies, normal rate (NOR), prophase apoptosis-like death rate (PADR), anaphase apoptosis-like death rate (AADR), necrosis rate (NER), intracellular calcium concentration ($[Ca^{2+}]_i$ concentration), mitochondrial membrane potential ($\Delta\Psi m$), reactive oxygen species (ROS), quantity of DNA fragmentations (QDF), caspase activities, and mRNA expression of apoptosis-related genes of *C. irritans* tomont were investigated to uncover the mechanism of honokiol for inducing *C. irritans* tomont apoptosis-like death.

Methods

Fish, drugs, and parasite

Trachinotus ovatus, weighing 80.0 ± 10.6 g, were purchased from a marine cage culture, Lingshui County, Hainan Province, P.R. China. The fish were soaked in seawater containing 1 ml/l formaldehyde for 10 min and acclimated in 2000 l aquaria for 21 days (diameter = 2 m, height = 1 m) equipped with aerators and a flow-through water system (water depth 0.6 m, water temperature 29.0 ± 2.0 ℃, pH 7.8 ± 0.2, salinity 30 ± 0.5, dissolved oxygen [DO] 6.8 ± 0.1 mg/l). The fish were fed marine fish feed (Zhongshan President Enterprises Co., Ltd., P.R. China) at 4% body weight three times (9:00, 16:00, and 22:00) every day.

Honokiol with a high-performance liquid chromatography (HPLC) purity ≥ 98% was purchased from Century Aoke Biological Technology Co., Ltd. (P.R. China). An amount of 250 mg of honokiol was dissolved in 25 ml 50% (v/v) ethanol aqueous solution and diluted to 800, 400, 200, 100, 60, and 0 (control sample) μg/ml with 50% (v/v) ethanol aqueous solution.

Cryptocaryon irritans used in this study were isolated from *T. ovatus* with white spot disease, which were obtained from a marine cage culture in Lingao County, Hainan Province, P.R. China, and passaged and propagated in *T. ovatus* [31]. All *C. irritans* tomonts used in this study were newly collected between 8:00 a.m. and 9:00 a.m. on the day of the experiment.

Experiment design

Cryptocaryon irritans tomonts were collected, resuspended in 1 ml filter-sterilized seawater, and added to the assigned wells in a 24-well microplate. Then, 10 μl of 0 (control sample), 60, 100, 200, 400, and 800 μg/ml honokiol 50% (v/v) ethanol aqueous solutions were added to the assigned wells in the 24-well microplates, respectively. The final honokiol concentrations were 0.0 (control sample), 0.6, 1.0, 2.0, 4.0, and 8.0 μg/ml, respectively. The 24-well microplates were placed in a light incubator (GZX250E, Tianjin Taisite Instrument Co., Ltd., P.R. China) at 27 ± 0.5 °C for 8 h. The morphologies, NOR, PADR, AADR, NER, $[Ca^{2+}]_i$ concentration, $\Delta\Psi m$, ROS, QDF, and caspase activities of the above-treated *C. irritans* tomonts were analyzed using a direct microscopic observation method, an Annexin V-FITC/PI apoptosis detection kit, a Fluo-3 AM calcium concentration detection kit, a mitochondrial membrane potential assay kit, a reactive oxygen species assay kit, a terminal deoxynucleotidyl transferase dUTP nick end labeling (TUNEL) apoptosis assay kit,

and a caspase-3/8/9 activity assay kit, respectively. *Cryptocaryon irritans* tomonts were treated with honokiol at the optimum concentration according to the results of the above experiments for 0, 1, 2, 4, 8, and 16 h. Their morphologies, NOR, PADR, AADR, NER, $[Ca^{2+}]_i$ concentration, $\Delta\Psi m$, ROS, QDF, and caspase activities were also analyzed using the same methods as mentioned above. *Cryptocaryon irritans* tomonts were treated with honokiol at the conditions with the highest apoptosis rate of tomonts according to the results of the above experiments, and then the inhibition rate of tomonts hatching was observed according to the method described by Zhong et al. [31]. Each well assigned to caspase activity analysis and the mRNA expression of apoptosis-related genes analysis contained 1000 *C. irritans* tomonts, while each well assigned to the other analyses contained 100 *C. irritans* tomonts. Each analysis was carried out five times in parallel.

Morphology observation and Annexin V-FITC/PI stain

The NOR, PADR, AADR, and NER of *C. irritans* tomonts were analyzed using an Annexin V-FITC/PI apoptosis detection kit (Beijing Solarbio Science & Technology Co., Ltd., P.R. China). The *C. irritans* tomonts, treated as described in "Experiment Design," were washed twice with 1 ml ice-cold PBS (pH = 7.4, 0.01 mol/l) and resuspended in 100 µl binding buffer. A solution of 5 µl Annexin V-FITC was added, and the tomonts were incubated at 27 ± 0.5 ℃ in the dark for 10 min. Then, a solution of 5 µl PI was added, and the tomonts were incubated at 27 ± 0.5 ℃ in the dark for 5 min, washed twice with 1 ml ice-cold PBS, and transferred to 384-well microplates (each well contained a *C. irritans* tomont). A total of 150 *C. irritans* tomonts were analyzed in parallel with a fluorescence microplate reader (BioTek Synergy H1, BioTek Instruments, Inc., USA) at Ex/Em = 488/525 nm and Ex/Em = 488/630 nm, and their micromorphologies were observed under a fluorescence inversion microscope (DMi8 + DFC7000T, Leica Microsystems, Germany). Four-quadrant apoptosis diagrams were drawn using a logarithm transformed Annexin V-FITC fluorescence intensity [LG ($A_{Ex/Em = 488/525\ nm}$)] as the abscissa axis and a logarithm transformed PI fluorescence intensity [LG ($A_{Ex/Em = 488/630\ nm}$)] as the ordinate axis. Normal (in the I quadrant), prophase apoptosis-like death (in the II quadrant), anaphase apoptosis-like death (in the III quadrant), and necrosis (in the IV quadrant) *C. irritans* tomonts were identified according to the four-quadrant apoptosis diagrams, and their numbers were recorded [28]. Finally, the percentages of the NOR, PADR, AADR, NER, and *C. irritans* tomonts were calculated.

$[Ca^{2+}]_i$ concentration determination

The $[Ca^{2+}]_i$ concentrations in *C. irritans* tomonts were determined using a Fluo-3 AM calcium concentration detection kit (Beijing Solarbio Science & Technology Co., Ltd., P.R. China). The *C. irritans* tomonts, treated as described in "Experiment Design," were washed twice with 1 ml PBS (pH = 7.4, 0.01 mol/l) and incubated in 200 µl Fluo-3 AM reaction mix (5 µmol/l) at 27 ± 0.5 ℃ in the dark for 20 min. Then, 1 ml 1% fetal bovine serum-Hank's balanced salt solution (HBSS, pH = 7.4, 0.01 mol/l) was added, and the tomonts were incubated at 27 ± 0.5 ℃ in the dark for 40 min, washed twice with 1 ml 2-[4-(2-hydroxyethyl)-1-piperazinyl] ethanesulfonic acid buffer (HEPES, pH = 7.4, 0.01 mol/l), and resuspended in 100 µl HEPES at 27 ± 0.5 ℃ in the dark for 10 min. The fluorescence intensity was determined using a fluorescence microplate reader (BioTek Synergy H1, BioTek Instruments, Inc., USA) at Ex/Em = 488/525 nm. The results were expressed as the total fluorescence intensity per 100 *C. irritans* tomonts.

$\Delta\Psi m$ determination

The $\Delta\Psi m$ in *C. irritans* tomonts was determined using a mitochondrial membrane potential assay kit with JC-1 (Beijing Solarbio Science & Technology Co., Ltd., P.R. China). The *C. irritans* tomonts were treated with carbonyl cyanide 3-chlorophenylhydrazone (CCCP, 10 µmol/l) for 20 min as a positive control. The *C. irritans* tomonts, treated as described in "Experiment Design" and with CCCP, were washed twice in 1 ml PBS (pH = 7.4, 0.01 mol/l), incubated in 10 µg/ml JC-1 reaction mix for 20 min at 27 ± 0.5 ℃ in the dark, washed twice with 1 ml JC-1 buffer solution (1×), and resuspended in 100 µl JC-1 binding buffer (1×). The fluorescence intensity was determined using a fluorescence microplate reader (BioTek Synergy H1, BioTek Instruments, Inc., USA) at Ex/Em = 490/530 nm and Ex/Em = 525/590 nm. The results were expressed as the rate of mitochondrial membrane potential polymer to monomer (polymer/monomer) per 100 *C. irritans* tomonts [32].

ROS determination

The ROS accumulation in *C. irritans* tomonts was determined by a reactive oxygen species assay kit (Beijing Solarbio Science & Technology Co., Ltd., P.R. China). The *C. irritans* tomonts, treated as described in "Experiment Design," were washed twice in 1 ml PBS (pH = 7.4, 0.01 mol/l), incubated in 200 µl 2',7'-dichlorodihydrofluorescein diacetate (DCFH-DA, 10 µmol/l) reaction mix at 27 ± 0.5 ℃ in the dark for 20 min, washed twice in 1 ml PBS (pH = 7.4, 0.01 mol/l), and resuspended in 100 µl PBS (pH = 7.4, 0.01 mol/l). The fluorescence intensity

was determined using a fluorescence microplate reader (BioTek Synergy H1, BioTek Instruments, Inc., USA) at Ex/Em = 488/525 nm. The results were expressed as the total fluorescence intensity per 100 *C. irritans* tomonts.

TUNEL assay

The QDF in *C. irritans* tomonts was determined using a TUNEL apoptosis assay kit (Beijing Solarbio Science & Technology Co., Ltd., P.R. China). The *C. irritans* tomonts, treated as described in "Experiment Design," were washed twice in 1 ml PBS (pH = 7.4, 0.01 mol/l), fixed in 200 µl 4% (w/v) paraformaldehyde at room temperature for 30 min, washed three times in 1 ml PBS (pH = 7.4, 0.01 mol/l), permeabilized with 200 µl 0.01% Triton-PBS (pH = 7.4, 0.01 mol/l) in ice for 2 min, washed twice in 1 ml PBS (pH = 7.4, 0.01 mol/l), and incubated in 100 µl TUNEL reaction mix (1×) at 27 ± 0.5 ℃ in the dark for 60 min, washed twice in 1 ml PBS (pH = 7.4, 0.01 mol/l), and resuspended in 100 µl PBS (pH = 7.4, 0.01 mol/l). The fluorescence intensity was determined using a fluorescence microplate reader (BioTek Synergy H1, BioTek Instruments, Inc., USA) at Ex/Em = 550/590 nm. The results were expressed as the total fluorescence intensity per 100 *C. irritans* tomonts.

Caspase activity determination

The activities of caspases, including caspase-3/8/9 in the *C. irritans* tomonts, were respectively determined using a caspase-3/8/9 activity assay kit (Beijing Solarbio Science & Technology Co., Ltd., P.R. China). On ice, the *C. irritans* tomonts, treated as described in "Experiment Design," were washed twice in 1 ml ice-cold PBS (pH = 7.4, 0.01 mol/l), a lysis buffer was added at a ratio of 1: 10 (*C. irritans* tomonts mass: lysis buffer, g:ml), ground to homogenate on the ice using a grinding rod, cracked in ice for 15 min, and centrifugated (15000 g, 4 ℃, 15 min). The supernatants were then collected. The supernatants, caspase reaction buffer, and substrates (Asp-Glu-Val-Asp-p-nitroanilide for caspase-3 activity determination, N-acetyl-Ile-Glu-Thr-Asp-p-nitroanilide for caspase-8 activity determination, and Leu-Glu-His-Asp-p-nitroanilide for caspase-9 activity determination) were added to 96-well enzyme plates and incubated at 37 ℃ for 8 h, determined by microplate reader (BioTek Synergy H1, BioTek Instruments, Inc., USA) at 405 nm. The activities of caspase-3/8/9 were calculated using the following function:

$$\mathrm{Caspaseactivity}\left(U/mgProtein\right) = \frac{X \times V_1}{V_2 \times C_{protein} \times T}$$

where X is the result of the calculation of the absorbance at 405 nm in the caspase standard curve (µmol/l), V_1 is the total volume of the reaction system (µl), V_2 is the volume of the added supernatant (µl), T is the reaction time (h), and $C_{protein}$ is the total protein concentration in the supernatant (mg/ml) determined by the Bradford method [33].

Effects of honokiol on the mRNA expression of apoptosis-related genes

The *C. irritans* tomonts were treated with honokiol at the optimum concentration obtained according to the results of experiment design for 0, 1, 2, 4, 8, and 16 h, and the mRNA expression of the 61 apoptosis-related genes obtained by blast according to the *C. irritans* genome (SRX12890364, SRX12890363) [34] was analyzed using the RT-PCR method. Each well assigned to mRNA expression of apoptosis-related gene analysis contained 1000 *C. irritans* tomonts. Each analysis was carried out in triplicate. The 61 apoptosis-related genes and their primers designed by the Primer 3 plus software (https://www.primer3plus.com/) according to the primer design rules [70] are listed in Additional file 1: Table S1. The specificities of the primers used in this study were confirmed using BLAST tool (https://blast.ncbi.nlm.nih.gov/Blast.cgi). Eastep Super Total RNA Extraction LS1040 (Promega Corp., USA) was used according to the manufacturer's instructions to extract total RNA by the glass tissue homogenizer from the treated *C. irritans* tomonts, and DNase I (Promega Corp., USA) was used to digest the contaminating DNA. Then, agarose gel electrophoresis and an ultramicro spectrophotometer (NanoPhotometer NP80, IMPLEN GMBH, Germany) were used to ensure the quality of RNA, and the cDNA sequence was synthesized using Eastep RT Master MIX Kit LS2054 (Promega Corp., USA). The mRNA expressions were detected using the CFX96 Real-Time PCR Detection System (Bio-Rad, Hercules, CA, USA) with a 10 µl reaction mixture containing 5 µl (2×) Eastep qPCR Master Mix (Vazyme Biotech Co., Ltd., P.R. China), 1.0 µl cDNA template, 0.2 µl each primer (10 µmol/l), and 3.6 µl nuclease-free water. Each sample was tested in triplicate. The real-time PCR cycling conditions were as follows: 120 s 95 °C initial denaturation, 40 cycles of 15 s 95 °C denaturation, and 60 s 60 °C annealing/extension. Dissociation curve analysis (65 to 95 °C: increment 0.5 °C for 5 s) was performed to verify the amplification of a single product. The *C. irritans* 18S rRNA gene sequence (JN636814.1) was used as the internal reference gene. Furthermore, the specificities of the primers were confirmed by the fluorescence quantitative melting curve used the CFX96 Real-Time PCR Detection System (Bio-Rad, Hercules, CA, USA). After real-time PCR, the mRNA expression of the apoptosis-related genes was calculated u the method of $2^{-\triangle\triangle Ct}$.

Statistical analysis

All the experimental indexes were tested using Tukey's test with SPSS 25.0 (IBM Corp., USA) to determine the significant difference between the experimental sample and the control sample. A difference was considered significant when the p values were < 0.05 and extremely significant when the p values were < 0.01. The chart was plotted using OriginPro 9.0 (OriginLab Corp., USA), and the data were expressed as mean ± standard deviation (SD).

Results

Results of morphology observation and Annexin V-FITC/PI stain

The morphologies of the unstained and AnnexinV-FITC/PI-stained *C. irritans* tomonts treated with honokiol are given in Fig. 1, showing that all the honokiol-treated *C. irritans* tomonts' cytoplasms obviously shrank, their cell membranes were separated from cysts, and they were stained with Annexin V-FITC (showing green fluorescence) in a dose-dependent manner; this indicates phosphatidylserine valgus in cell membrane (a typical cell apoptosis characteristic). When the concentration of honokiol was > 4.0 μg/ml, the treated *C. irritans* tomonts' cytoplasms were irregularly condensed, became hyaline, and were stained by PI (showing red fluorescence), which indicates their cell membranes were damaged (a typical characteristic of middle- and late-stage cell apoptosis or necrosis). Four-quadrant apoptosis diagrams are given in Fig. 2, showing that with the increase in honokiol, the PADR began to increase at a concentration of 0.6 μg/ml. It reached its highest level when the honokiol concentration was 1.0 μg/ml and then decreased, while the AADR and NER began to increase at a concentration of 2.0 μg/ml.

Effect of honokiol on $[Ca^{2+}]_i$ concentration, ΔΨm, ROS, QDF, and caspase-3/8/9 activities

The $[Ca^{2+}]_i$ concentration and the ΔΨm, ROS, QDF, and caspase-3/8/9 activities in the *C. irritans* tomonts treated with honokiol at various concentrations are given in Fig. 3. As shown in Fig. 3A, with the increase in the honokiol concentration, the $[Ca^{2+}]_i$ concentration increased to a level significantly higher than that of the control sample at 0.6 μg/ml. It reached the highest level at 1 μg/ml, returned to the level of the control sample

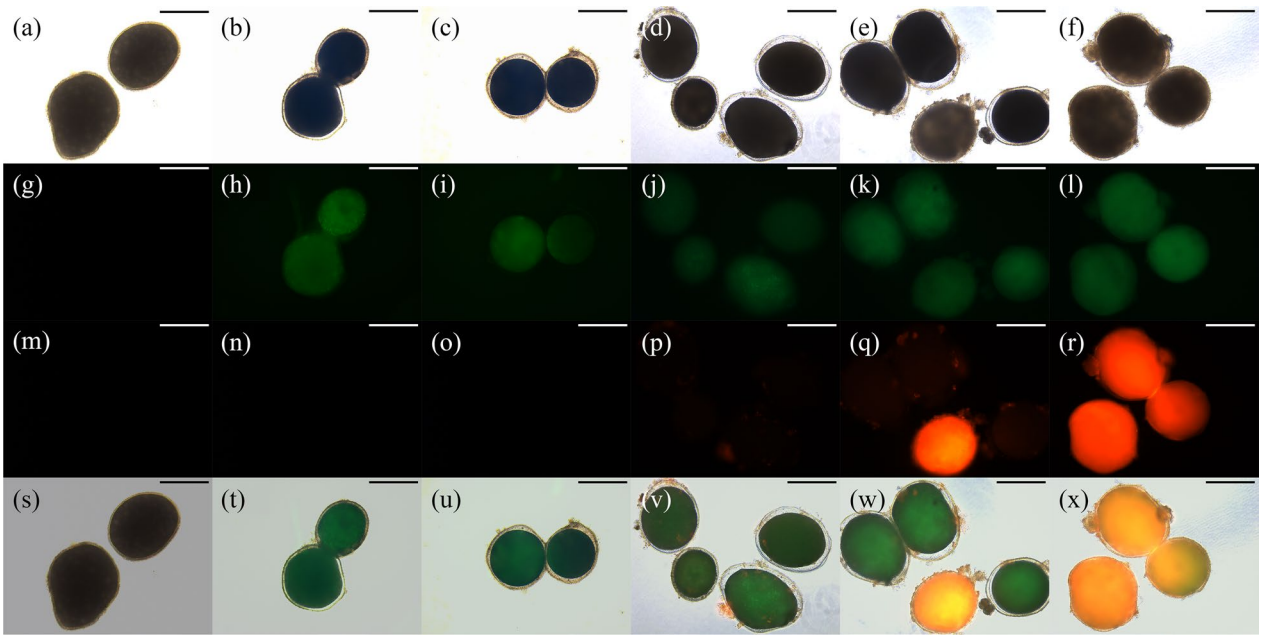

Fig. 1 Morphologies of honokiol-treated *Cryptocaryon irritans* tomonts stained and unstained with Annexin V-FITC/PI. The *C. irritans* tomonts were treated with honokiol at 0.0, 0.6, 1.0, 2.0, 4.0, and 8.0 μg/ml for 8 h. The treated tomonts were incubated with Annexin V-FITC and a PI probe and observed under a fluorescence inversion microscope (DMi8 + DFC7000T, Leica Microsystems, Germany). The results show that all the honokiol-treated *C. irritans* tomonts' cytoplasms obviously shrank and were stained with Annexin V-FITC. When the concentration of honokiol was > 4.0 μg/ml, the treated *C. irritans* tomonts' cytoplasms were irregularly condensed, became hyaline, and were stained by PI. **a**–**f**: Morphologies of *C. irritans* tomonts respectively treated with 0.0, 0.6, 1.0, 2.0, 4.0, and 8.0 μg/ml honokiol for 8 h. **g**–**l**: Morphologies of *C. irritans* tomonts respectively treated with 0.0, 0.6, 1.0, 2.0, 4.0, and 8.0 μg/ml honokiol for 8 h and observed at Ex/Em = 488/525 nm. **m**–**r**: Morphologies of *C. irritans* tomonts respectively treated with 0.0, 0.6, 1.0, 2.0, 4.0, and 8.0 μg/ml honokiol for 8 h and observed at Ex/Em = 488/630 nm. **s**–**x**: Overlapping morphology photos of *C. irritans* tomonts respectively treated with 0.0, 0.6, 1.0, 2.0, 4.0, and 8.0 μg/ml honokiol for 8 h and recorded at Ex/Em = 488/525 nm and Ex/Em = 488/630 nm. All bars = 300 μm

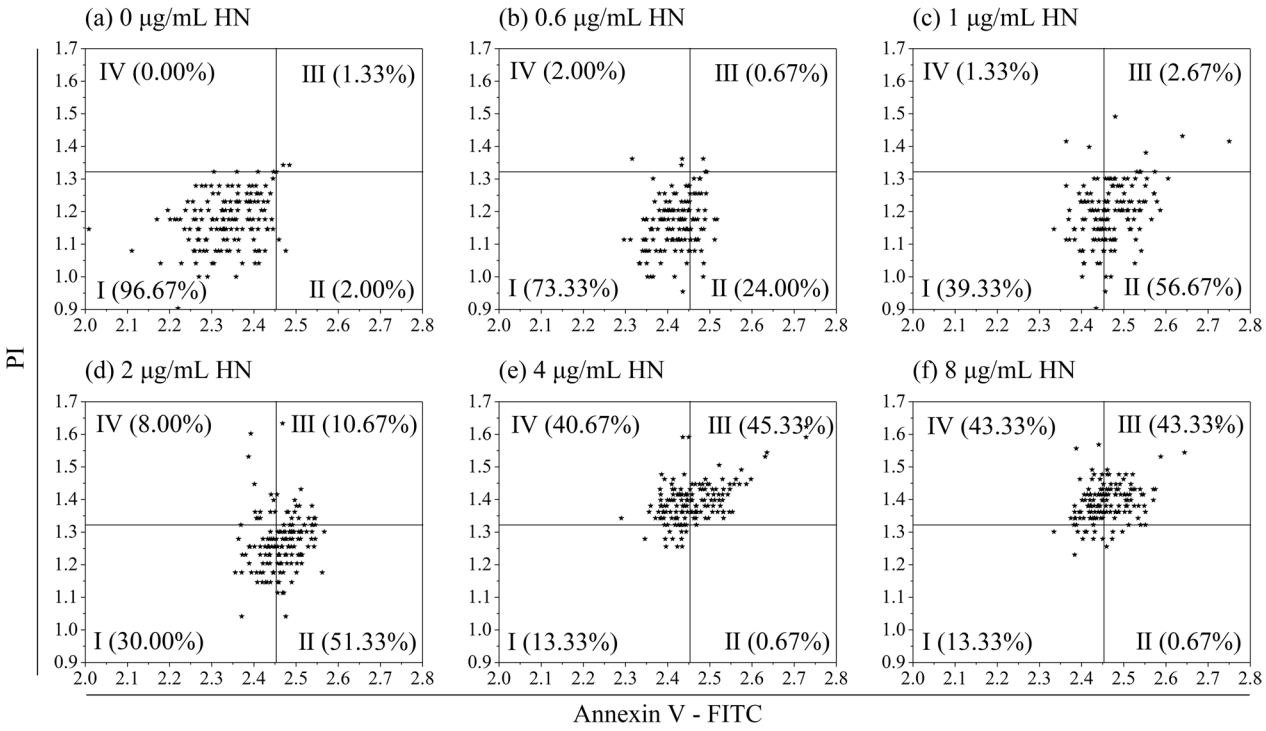

Fig. 2 Four-quadrant apoptosis diagrams of *Cryptocaryon irritans* tomonts treated with honokiol at various concentrations for 8 h. The *C. irritans* tomonts were treated with honokiol at 0.0, 0.6, 1.0, 2.0, 4.0, and 8.0 μg/ml for 8 h. The treated tomonts were incubated with Annexin V-FITC and a PI probe and analyzed with a fluorescence microplate reader (BioTek Synergy H1, BioTek Instruments, Inc., USA). The results show that with the increase in honokiol concentration, the PADR began to increase at 0.6 μg/ml and reached the highest level at 1.0 μg/ml, while the AADR and NER began to increase at 2.0 μg/ml

at 2.0 μg/ml, and then decreased to a level significantly lower than that of the control sample when the honokiol concentration increased > 4.0 μg/ml. As shown in Fig. 3B, the $\Delta\Psi$m decreased to a level significantly lower than that of the control sample when the honokiol concentration was > 0.6 μg/ml. As shown in Fig. 3C, with the increase of the honokiol concentration, the ROS increased to a level significantly higher than that of the control sample at 1.0 μg/ml and then returned to the level of the control sample. As Fig. 3D shows, with the increase of the honokiol concentration, the QDF began to increase at 0.6 μg/ml, increased to a level significantly higher than that of the control sample at 1.0 μg/ml, reached the highest level at 2.0 μg/ml, and then decreased, but the level remained significantly higher than that of the control sample when the honokiol concentration increased above 4.0 μg/ml. As shown in Fig. 3E, with the increase of the honokiol concentration, both the caspase-3/9 activities began to increase to levels significantly higher than those of the control sample at 0.6 μg/ml and reached the highest levels at 1.0 μg/ml. The activity of caspase-3 gradually returned to the level of the control sample when the honokiol concentration was ≥ 4.0 μg/ml, while the activity of caspase-9 remained at a level higher than that of the control sample, and the activity of caspase-8 always remained at the level of the control sample.

Effects of honokiol treatment time on *C. irritans* tomont apoptosis-like death

The results found in "Effect of honokiol on $[Ca^{2+}]_i$ concentration, $\Delta\Psi$m, ROS, QDF, and caspase-3/8/9 activities" showed that *C. irritans* tomonts had the highest PADR, $[Ca^{2+}]_i$ concentration, ROS, caspase-3/9 activities, and higher QDF, and the lowest NER when the honokiol concentration was 1.0 μg/ml. Therefore, 1.0 μg/ml was considered the optimum honokiol concentration for inducing *C. irritans* tomont apoptosis-like death. Together with the extension of the treatment time, the changes in the NOR, PADR, AADR, NER, $[Ca^{2+}]_i$ concentration, $\Delta\Psi$m, ROS, QDF, and the caspase-3/8/9 activities for the *C. irritans* tomonts are given in Fig. 4, showing that, with the extension of the treatment time, the $[Ca^{2+}]_i$ concentration and PADR began to increase significantly at 1 h, followed by ROS and QDF. The caspase-3/9 activities began to increase significantly, and the $\Delta\Psi$m began to decrease significantly at 2 h. The $[Ca^{2+}]_i$ concentration, PADR, ROS, QDF, and caspase-3/9 activities reached the highest

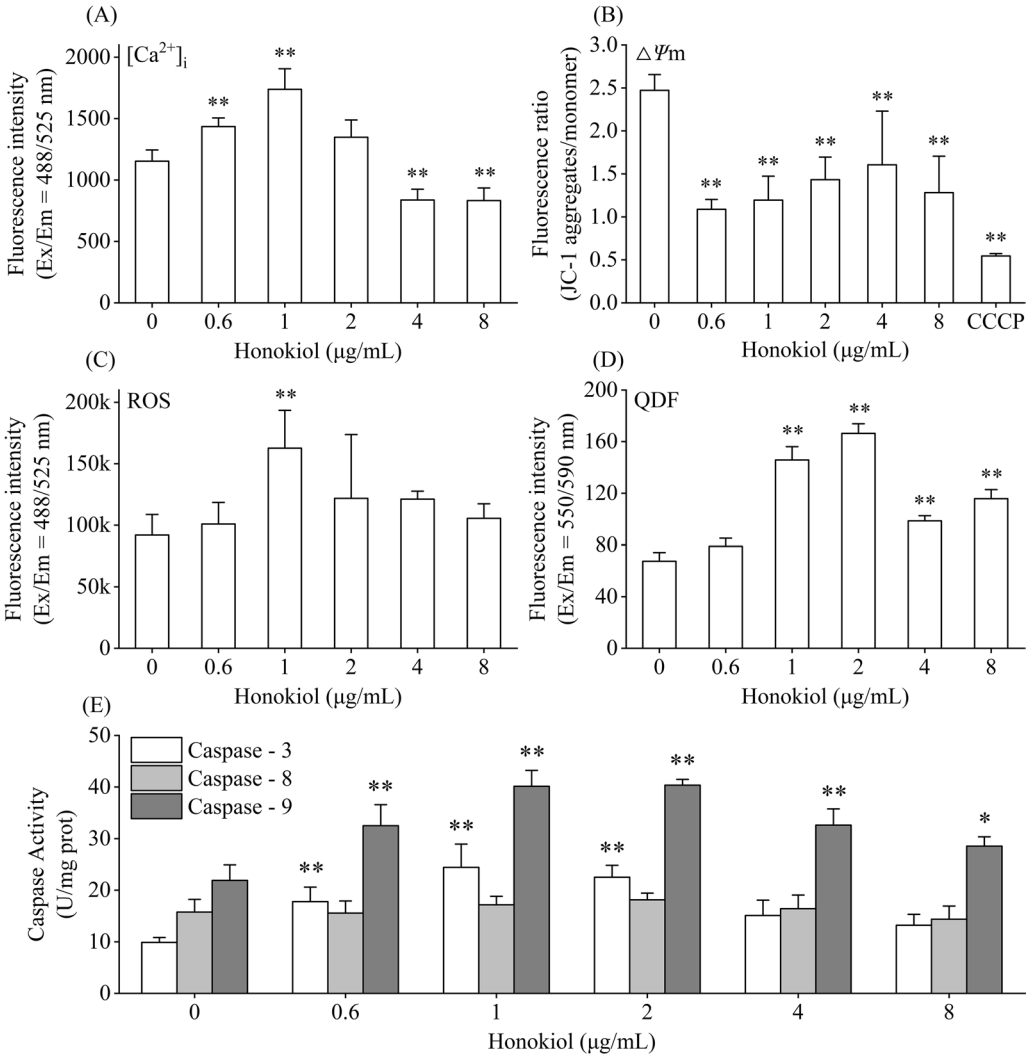

Fig. 3 Effects of the 8 h treatment of honokiol at various concentrations on the $[Ca^{2+}]_i$ concentration, ΔΨm, ROS, QDF, and caspase-3/8/9 activities in *Cryptocaryon irritans* tomonts. The *C. irritans* tomonts were treated with honokiol at 0.0, 0.6, 1.0, 2.0, 4.0, and 8.0 μg/ml for 8 h, and the $[Ca^{2+}]_i$ concentration, ΔΨm, ROS, QDF, and caspase-3/8/9 activities were determined. The results show that the $[Ca^{2+}]_i$ concentration, ΔΨm, ROS, and the caspase-3/9 activities all reached the highest significant levels when the honokiol was 1.0 μg/ml, and the QDF reached the highest significant level when the honokiol was 2.0 μg/ml. **a** Effect of honokiol on $[Ca^{2+}]_i$ concentration in *C. irritans* tomonts. **b** Effect of honokiol on ΔΨm in *C. irritans* tomonts. **c** Effect of honokiol on ROS in *C. irritans* tomonts. **d** Effect of honokiol on QDF in *C. irritans* tomonts. **e** Effect of honokiol on caspase-3/8/9 activities in *C. irritans* tomonts. The results are expressed as mean ± SD, $n = 5$. *Significant difference from the control sample (0.0 μg/ml), $P < 0.05$. **Highly significant difference from the control sample (0.0 μg/ml), $P < 0.01$

levels at 4 h and then slightly decreased but remained at levels significantly higher than those at 0 h, while the ΔΨm continued to decrease at 16 h, and the AADR began to significantly increase at 8 h. The NER and the activity of caspase-8 showed nonsignificant changes at 16 h. These results suggest that the optimum treatment time for 1.0 μg/ml honokiol inducing *C. irritans* tomonts apoptosis-like death is 4 h. The inhibition rate

(See figure on next page.)

Fig. 4 Effect of honokiol treatment time on *Cryptocaryon irritans* tomont apoptosis-like death. The *C. irritans* tomont treated with 1 μg/ml honokiol at 0, 1, 2, 4, 8, and 16 h and their NOR, PADR, AADR, NER, $[Ca^{2+}]_i$ concentration, ΔΨm, ROS, QDF, and caspase-3/8/9 activities were determined. The result shows that the $[Ca^{2+}]_i$ concentration began to increase significantly at 1 h, and then the ROS, QDF, and caspase-3/9 activities began to increase significantly and the ΔΨm began to decrease significantly at 2 h; the highest PADR was obtained at 4 h. The results are expressed as mean ± SD, $n = 5$. *Significant difference from the control sample (0.0 μg/ml), $P < 0.05$. **Highly significant difference from the control sample (0.0 μg/ml), $P < 0.01$

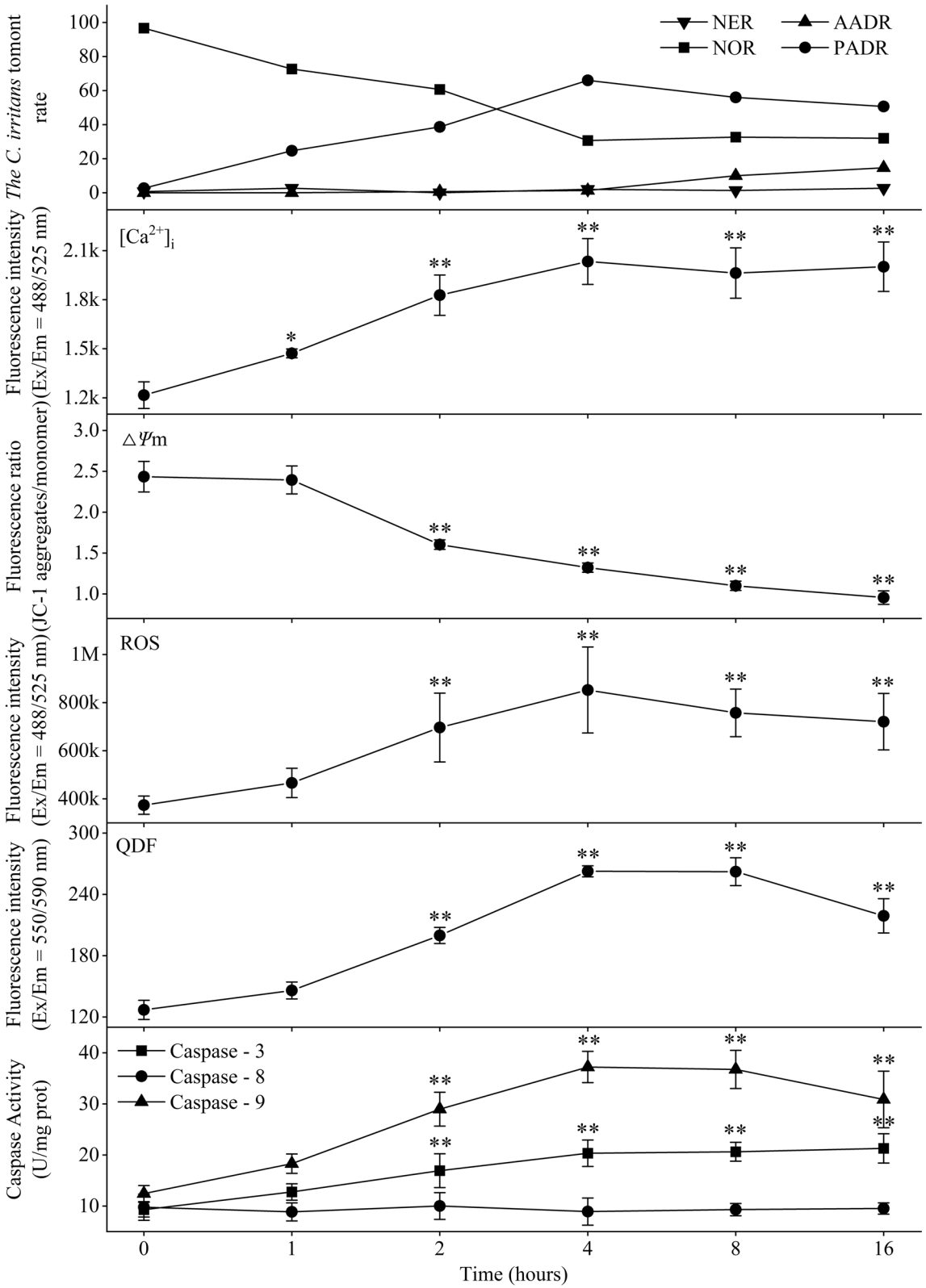

Fig. 4 (See legend on previous page.)

of tomont hatching was 52.38% after treatment with 1.0 μg/ml honokiol for 4 h.

Effects of honokiol on the mRNA expression of apoptosis-related genes

Among the 61 investigated apoptosis-related genes, 14 were significantly upregulated (shown in Fig. 5). The fluorescence quantitative melting curves of the 14 genes are shown in Additional file 2: Fig. S1. Among the 14 upregulated genes, *itpr2*, *capn1*, *mc*, *actg1*, *actb*, *parp2*, *traf2*, and *fos* were enriched in the pathway related to apoptosis induced by the disruption of the $[Ca^{2+}]$ homeostasis in ER. Among the eight genes, *fos* was significantly upregulated at 4 h, while the other genes were significantly upregulated within 2 h. Gene *gzmb*, enriched in the Granzyme B pathway, was significantly upregulated at 16 h, and gene *tuba1c*, enriched downstream of the Granzyme B pathway, was significantly upregulated at 2 h. Genes *hras* and *raf1*, enriched in the MAPK signaling pathway, were significantly upregulated at 2 h, and gene *hras was* also significantly upregulated at 4 h. Gene *akt1*, enriched in the PI3K-Akt signaling pathway, was significantly upregulated at 2 h. Gene *atm*, the upstream regulatory of the p53 signaling pathway, was significantly upregulated at 2, 4, and 16 h.

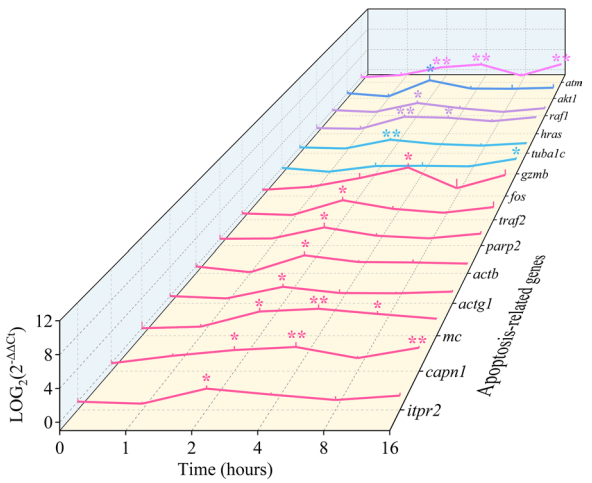

Fig. 5 mRNA expression of apoptosis-related genes in *Cryptocaryon irritans* tomonts treated with honokiol. The mRNA expression of the apoptosis-related genes in *C. irritans* tomonts were respectively treated with 1.0 μg/ml honokiol at 0, 1, 2, 4, 8, and 16 h. The results show that a total of 14 genes increased significantly at different times. The results are expressed as mean ± SD, $n = 3$. *Significant difference from the control (0.0 μg/ml), $P < 0.05$. **Highly significant difference from the control (0.0 μg/ml), $P < 0.01$

Discussion

The apoptosis-like death pathway has been found in many protozoa, such as Leishmania, *P. falciparum*, *T. thermophila*, *T. cruzi*, *B. hominis*, *T. gondii,* and *I. multifiliis* [12–21]. *Ichthyophthirius multifiliis* is the pathogen of freshwater white spot disease, the morphology and life cycle of which are similar to those of *C. irritans* [1]. It has been reported that fish skin antibodies could cause *I. multifiliis* apoptosis-like phenomena, such as PS externalization and chromatin condensation [16]. It has also been reported that malachite green could cause *I. multifiliis* apoptosis-like phenomena, such as mitochondrial swelling, mitochondrial membrane integrity destruction, ribosome number change, and PS externalization through the PI3K-Akt signal pathway [21]. In this study, honokiol was demonstrated to cause significant *C. irritans* tomont cytoplasm atrophy, cell volume reduction, PS externalization, a significant increase in QDF, $[Ca^{2+}]_i$ concentration, ROS and caspase-3/9 activities, a significant decrease in $\Delta\Psi m$, and significant upregulation of the mRNA expression of the 14 apoptosis-related genes; this strongly suggests that *C. irritans* tomonts have a form of regulated apoptosis-like death. The apoptosis-like death named by the Nomenclature Committee on Cell Death (NCCD) resembles the apoptosis of metazoans [35] and has been considered an ideal strategy to prevent and treat parasitic diseases [11, 36]. Although this study has proved that apoptosis-like death exists in *C. irritans* tomonts, which provides a potential new way to treat marine fish white spot disease with the advantages of a lower probability of drug resistance and adverse effects, further studies are needed to uncover and confirm the mechanism of honokiol inducing *C. irritans* tomont apoptosis-like death.

Honokiol, as one of the main active components of *M. officinalis*, has been reported to induce apoptosis of several cells, such as neuroblastoma cells, A549 cells, 95-D cells, and human chondrosarcoma cells, fungi such as *C. albicans*, and protozoan parasites such as Leishmania via the ER stress pathway [8, 27–30, 36–39]. The reported ER stress pathway inducing cell apoptosis is summarized in Fig. 6, which shows that drugs such as honokiol and physiological or environmental factors can cause excessive or aberrant ER stress [30, 40–42]. Excessive or aberrant ER stress leads to Ca^{2+} release from ER via the inositol 1,4,5-trisphosphate receptor (IP3Rs) and to unfolded protein response (UPR) accumulation [43–47]. Cho et al. [48] reported that honokiol could promote $[Ca^{2+}]_i$ release and increase $[Ca^{2+}]_i$ concentration by inhibiting the activity of endoplasmic reticulum protein 44 (ERP44), which has inhibitory activity on the calcium channel IP3Rs [49]. Similarly, the $[Ca^{2+}]_i$ concentration first significantly increased in *C. irritans* tomonts in this

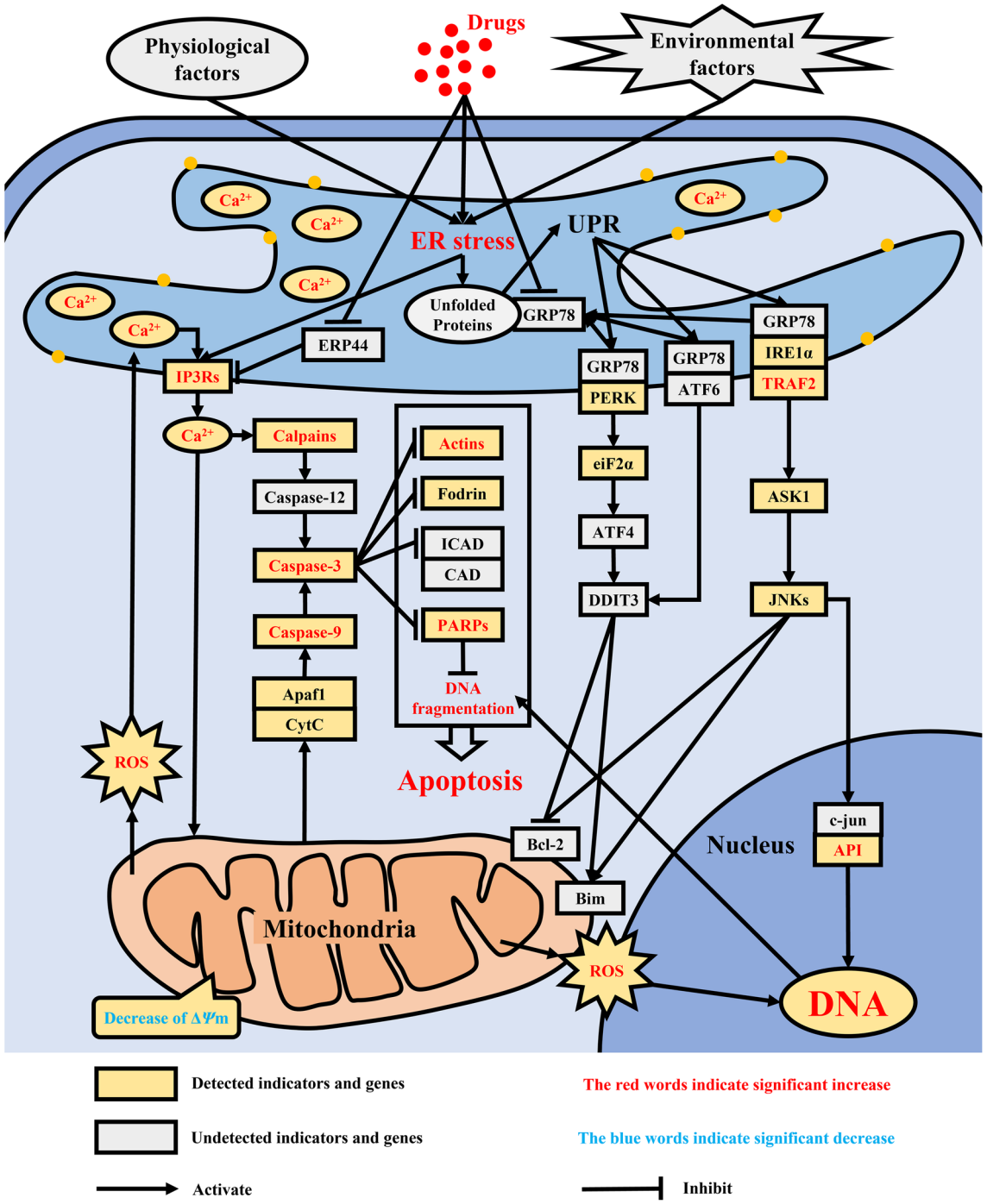

Fig. 6 Regulatory mechanism of apoptosis induced by ER stress. This figure shows that the classic ER stress pathway induces cell apoptosis. Apaf1, Cytc, Fodrin, PERK, eiF2α, IRE1α, TRAF2, ASK1, and API were coded with *apaf1*, *cycs*, *sptan1*, *eif2ak3*, *eif2s1*, *ern1*, *traf2*, *map3k5*, and *fos*, respectively. Beta-actin and γ-actin were respectively coded with *actb* and *actg1*. Calpains included the calpain-1 catalytic subunit and the calpain-2 catalytic subunit, which were coded with *capn1* and *capn2*. PARPs include poly [ADP-ribose] polymerase 2 and poly [ADP-ribose] polymerase 4, which were coded with *parp2* and *parp4*. JNKs include mitogen-activated protein kinase 9 and mitogen-activated protein kinase 10, which were respectively coded with *mapk9* and *mapk10*. IP3Rs include inositol 1,4,5-trisphosphate receptor type 2 and inositol 1,4,5-trisphosphate receptor type 3, which were respectively coded with *itpr1*, *itpr2*, and *itpr3*. The mRNA expression of *itpr2*, *capn1*, *mc*, *actg1*, *actb*, *parp2*, *traf2*, and *fos* increased significantly in this study

study. The increase of Ca^{2+} can cause two significant reactions, Reaction I and Reaction II. In Reaction I, the increase of Ca^{2+} can provoke the cascade reaction of caspases, including calpains, caspase-12, and caspase-3 [50–52]. Coinciding with Reaction I, the mRNA expression of gene *capn1* coding calpain was significantly upregulated and the activity of caspase-3 significantly increased in *C. irritans* tomonts. Via blasting in the *C. irritans* genome, gene *caspase-12* coding caspase-12 was not found, but gene *mc* coding metacaspase was found, and its mRNA expression was also significantly upregulated. Metacaspase has been reported to have an apoptosis regulation function in protozoa such as Leishmania and Plasmodium, which is similar to caspase-12 in metazoa [11, 53, 54]. In Reaction II, the increase of $[Ca^{2+}]_i$ can also decrease the $\Delta\Psi m$ of mitochondria and then promote ROS production and release from mitochondria [44, 55, 56]. An increase in ROS can further promote $[Ca^{2+}]_I$ release and increase QDF, and then the mitochondria sequentially activate caspase-9 and caspase-3 via apoptotic protease-activating factor 1 (Apaf1) combined with cytochrome c (CytC) [45, 57]. In agreement with Reaction II, honokiol has been proven to significantly decrease $\Delta\Psi m$ of mitochondria and increase ROS production, the activities of caspase-9 and caspase-3, and QDF in *C. irritans* tomonts. The activated caspase-3 can hydrolyze and deactivate actins and poly ADP-ribose polymerase (PARPs) [58–60]. Actins are involved in the maintenance of the cytoskeleton. Therefore, hydrolyzed actins cause cytoplasm atrophy and cell volume reduction [61–63], while hydrolyzed PARPs cause irreversible DNA damage and QDF increase [64–66]. In supporting these phenomena, this article has proven that honokiol could significantly upregulate the mRNA expressions of genes *actg1*, *actb*, and *parp2*, which respectively code actins and PARPs, cause *C. irritans* tomont cytoplasm atrophy and cell volume reduction, and increase the QDF [67–69]. Besides this apoptosis pathway, caused by ER stress via Ca^{2+}, the ER stress also leads to the accumulation of UPR. Under homeostatic conditions, proteins involved in the UPR, protein kinase RNA-like endoplasmic reticulum kinase (PERK), activating transcription factor 6 (ATF6), and inositol-requiring enzyme 1α (IRE1α) are bound to glucose-regulated protein 78 (GRP78) by their ER lumen domains, keeping them inactive. With the accumulation of UPR, causing GRP78 to leave PERK, ATF6, and IRE1α, the activation of these proteins is induced [45–47] (Fig. 6). The activated PERK activates the cascade reaction, including eukaryotic translation initiation factor 2 subunit alpha (eiF2α), activating transcription factor 4 (ATF4), and DNA damage inducible transcript 3 (DDIT3). DDIT3 can decrease the expression of anti-apoptosis proteins such as B-cell lymphoma 2 (Bcl-2) and increase the expression of pro-apoptosis proteins such as Bcl-2 interacting mediator of cell death (Bim). Then, the mitochondria sequentially activate caspase-9 and caspase-3 via Apaf1 combined with CytC. Finally, cell apoptosis is induced [46]. The activated ATF6 also activates DDIT3 and induces apoptosis via the mitochondria pathway. The activated IRE1α, combined with TNF receptor-associated factor 2 (TRAF2), activates cascade reactions, including apoptosis signal-regulating kinase 1 (ASK1) and c-jun n-terminal kinase (JNKs). JNKs are responsible for phosphorylation of the mitochondrial proteins Bim (pro-apoptosis) and Bcl2 (anti-apoptosis), which are activated and inhibited, respectively. Then, the activated JNKs induce the mitochondria apoptosis pathway or upregulate the expression of the jun proto-oncogene (c-jun) and fos proto-oncogene (API), increase the QDF, and induce cell apoptosis [45–47]. Although the mRNA expressions of *traf2* and *fos* in this pathway were significantly upregulated by honokiol, those of *eif2ak3*, *eif2s1*, *ern1*, *map3k5*, *mapk9*, and *mapk10* showed nonsignificant changes when *C. irritans* tomonts were treated with honokiol. This suggests that honokiol might not induce *C. irritans* tomont apoptosis via this pathway. In summary, the results of this study suggest that honokiol might inhibit the activity of ERP44 and unlimited IP3R release $[Ca^{2+}]_i$, disrupt $[Ca^{2+}]_i$ homeostasis in ER, and then induce *C. irritans* tomont apoptosis-like death by caspase cascade or mitochondrial pathway. However, further studies such as the transcriptomic or proteomic analyses are needed to confirm this suggestion.

Conclusion

This article showed that honokiol can induce *C. irritans* tomont apoptosis-like death and suggested that honokiol may disrupt $[Ca^{2+}]_i$ homeostasis in ER and then induce *C. irritans* tomont apoptosis-like death by caspase cascade and mitochondrial pathway. This might represent a novel therapeutic intervention for *C. irritans* infection. Next, to further research on safe and efficient anti-*C. irritans* drugs, the intracellular target of honokiol in *C. irritans* needs to be verified.

Abbreviations

C. irritans	*Cryptocaryon irritans*
ER	Endoplasmic reticulum
NOR	Normal rate
PADR	Prophase apoptosis-like death rate
AADR	Anaphase apoptosis-like death rate
NER	Necrosis rate
$[Ca^{2+}]_i$ concentration	Intracellular calcium concentration
$\Delta\Psi m$	Mitochondrial membrane potential
ROS	Reactive oxygen species
QDF	Quantity of DNA fragmentations
IP3Rs	Inositol 1,4,5-trisphosphate receptor
UPR	Unfolded protein response
ERP44	Endoplasmic reticulum protein 44

Apaf1	Apoptotic protease-activating factor 1
CytC	Cytochrome c
PARPs	Poly ADP-ribose polymerase
PERK	Protein kinase RNA-like endoplasmic reticulum kinase
ATF6	Activating transcription factor 6
IRE1α	Inositol-requiring enzyme 1α
GRP78	Glucose-regulated protein 78
eiF2α	Eukaryotic translation initiation factor 2 subunit alpha
ATF4	Activating transcription factor 4
DDIT3	DNA damage inducible transcript 3
Bcl-2	B-cell lymphoma 2
Bim	Bcl-2 interacting mediator of cell death
TRAF2	TNF receptor-associated factor 2
ASK1	Apoptosis signal-regulating kinase 1
JNKs	C-jun n-terminal kinase
c-jun	Jun proto-oncogene
API	Fos proto-oncogene

Supplementary Information

The online version contains supplementary material available at https://doi.org/10.1186/s13071-023-05910-1.

Additional file 1: Table S1. The 61 apoptosis-related genes and their primers used in this study.

Additional file 2: Fig. S1. The fluorescence quantitative melting curves of the 14 significantly differentially expressed genes.

Acknowledgements
Not applicable.

Author contributions
WLG and ZCZ finished the conception and design of this study. ZCZ, MYJ, SLL and QQH finished the experiments of this study. YCZ, WLG and ZCZ finished the writing, editing and review of this article. JHH, HWD, CL and ZHZ finished the discussion and comments for this article. YCZ and WLG were overall in charge of this research.

Funding
This work was financially supported by the National Natural Science Foundation of China (no. 31960739), National Key Research and Development Program of China (2021YFC2600600), Hainan Province Science and Technology Special Fund (ZDKJ2021016), and the Special Foundation of Agricultural and Rural Bureau of Lingao County, Hainan, China (no. ZLHX2018-124R).

Availability of data and materials
The data supporting the conclusions of this article are included within the article.

Declarations

Ethics approval and consent to participate
The experiment complied with the eighth edition of the Guide for the Care and Use of Laboratory Animals (Committee for the Update of the Guide for the Care and Use of Laboratory Animals, 2011). It was authorized by the Hainan University Institutional Animal Use and Care Committee (HNUAUCC-2020-00002).

Consent for publication
All authors give consent for publication.

Competing interests
The authors declare that they have no competing interests.

Author details
[1]Hainan Provincial Key Laboratory for Tropical Hydrobiology and Biotechnology, College of Marine Science, Hainan University, Haikou 570228, People's Republic of China. [2]School of Life Sciences, Hainan University, Haikou 570228, People's Republic of China. [3]Aquaculture Department, Hainan Agriculture School, Haikou 571101, People's Republic of China. [4]Technology Center of Haikou Customs District, Haikou 570105, People's Republic of China.

Received: 26 May 2023 Accepted: 31 July 2023
Published online: 16 August 2023

References

1. Brown EM. A New Parasitic Protozoan, the Causal Organism of a White Spot Disease in Marine Fish *Cryptocaryon irritans* Gen at sp.n. Agenda Abstr. Sci Meet Zool Soc Lond. 1951;11:1–2.
2. Sun HY, Zhu XQ, Xie MQ, Wu XY, Li AX, Lin RQ, et al. Characterization of *Cryptocaryon irritans* isolates from marine fishes in Mainland China by ITS ribosomal DNA sequences. Parasitol Res. 2006;99:160–6.
3. Imajoh M, Morimitu K, Sukeda M, Umezaki T, Monno S, Goda H, et al. TaqMan real-time PCR detection and phylogenetic analysis of *Cryptocaryon irritans* in Nomi Bay, Kochi. Japan Fish Pathol. 2016;51:103–11.
4. Van KV, Nhinh DT. The prevalence of *Cryptocaryon irritans* in wild marine ornamental fish from Vietnam. IOP Conf Series: Earth Environ Sci. 2018;137:1755–1307.
5. Dan XM, Li AX, Lin XT, Teng N, Zhu XQ. A standardized method to propagate *Cryptocaryon irritans* on a susceptible host pompano *Trachinotus ovatus*. Aquaculture. 2006;258:127–33.
6. Galluzzi L, Vitale I, Aaronson SA, Abrams JM, Adam D, Agostinis P, et al. Molecular mechanisms of cell death: recommendations of the nomenclature committee on cell death 2018. Cell Death Differ. 2018;25:486–541.
7. Goldar S, Khaniani MS, Derakhshan SM, Baradaran B. Molecular mechanisms of apoptosis and roles in cancer development and treatment. Asian Pacific J Cancer Prev. 2015;16:2129–44.
8. Kim C, Kim B. Anti-cancer natural products and their bioactive compounds inducing ER stress-mediated apoptosis: a review. Nutrients. 2018;10:1021.
9. Sugiura R, Satoh R, Takasaki T. ERK: a double-edged sword in cancer ERK-dependent apoptosis as a potential therapeutic strategy for cancer. Cells. 2021;10:2509.
10. Fulda S. Targeting extrinsic apoptosis in cancer: challenges and opportunities. Semin Cell Dev Biol. 2015;39:20–5.
11. Basmaciyan L, Casanova M. Cell death in *Leishmania*. Parasite. 2019;26:71.
12. Gannavaram S, Debrabant A. Programmed cell death in *Leishmania*: biochemical evidence and role in parasite infectivity. Front Cell Infect Microbiol. 2012;2:95.
13. Reece SE, Pollitt LC, Colegrave N, Gardner A. The meaning of death: evolution and ecology of apoptosis in protozoan parasites. PLoS Pathog. 2011;7:e1002320.
14. Ch'ng JH, Kotturi SR, Chong AG, Lear MJ, Tan KS. A programmed cell death pathway in the malaria parasite *Plasmodium falciparum* has general features of mammalian apoptosis but is mediated by Clan CA cysteine proteases. Cell Death Dis. 2010;1:e26.
15. Tan KS, Howe J, Yap EH, Singh M. Do *Blastocystis hominis* colony forms undergo programmed cell death? Parasitol Res. 2001;87:362–7.
16. Xu DH, Klesius PH, Shoemaker CA. Cutaneous antibodies from channel catfish, *Ictalurus punctatus* (Rafinesque), immune to *Ichthyophthirius multifiliis* (Ich) may induce apoptosis of Ich Theronts. J Fish Dis. 2005;28:213–20.
17. Bruchhaus I, Roeder T, Rennenberg A, Heussler VT. Protozoan parasites: programmed cell death as a mechanism of parasitism. Trends Parasitol. 2007;23:376–83.
18. Ni Nyoman AD, Lüder CG. Apoptosis-like cell death pathways in the unicellular parasite *Toxoplasma gondii* following treatment with apoptosis inducers and chemotherapeutic agents: a proof-of-concept study. Apopt Int J Program Cell Death. 2013;18:664–80.
19. Ye Q, Zhang C, Wang Z, Feng Y, Zhou A, Xie S, et al. Induction of oxidative stress, apoptosis and DNA damage by Koumine in *Tetrahymena thermophila*. PLoS ONE. 2019;14:e0212231.
20. Bethencourt-Estrella CJ, Delgado-Hernández S, López-Arencibia A, San Nicolás-Hernández D, Sifaoui I, Tejedor D, et al. Acrylonitrile derivatives against *Trypanosoma cruzi*: in vitro activity and programmed cell death study. Pharmaceuticals. 2021;14:552.

21. Qu S, Song C, Tan X, Wang G, Ling F. Comparative proteomic analysis provides insight into the key proteins as potential targets underlying the effect of malachite green against *Ichthyophthirius multifiliis*. J Fish Dis. 2021;44:881–92.
22. Lokanathan Y, Mohd-Adnan A, Wan KL, Nathan S. Transcriptome Analysis of the *Cryptocaryon irritans* tomont stage identifies potential genes for the detection and control of cryptocaryonosis. BMC Genomics. 2010;11:76.
23. Mo ZQ, Li YW, Wang HQ, Wang JL, Ni LY, Yang M, et al. Comparative transcriptional profile of the fish Parasite *Cryptocaryon irritans*. Parasit Vectors. 2016;9:630.
24. Yin F, Sun P, Wang J, Gao Q. Transcriptome analysis of dormant tomonts of the marine fish ectoparasitic ciliate *Cryptocaryon irritans* under low temperature. Parasit Vectors. 2016;9:280.
25. Chen R, Mao Y, Wang J, Liu M, Qiao Y, Zheng L, et al. Molecular mechanisms of an antimicrobial peptide piscidin (Lc-pis) in a parasitic protozoan. Cryptocaryon Irritans BMC Geno. 2018;19:192.
26. Chi H, Goldstein M, Pichardo A, Wei ZH, Chang WJ, Gong H. Infectivity and genes differentially expressed between young and aging theront cells of the marine fish parasite *Cryptocaryon irritans*. PLoS ONE. 2020;15:e0238167.
27. Deng J, Qian Y, Geng L, Chen J, Wang X, Xie H, et al. Involvement of p38 mitogen-activated protein kinase pathway in honokiol-induced apoptosis in a human hepatoma cell line (hepG2). Liver Int. 2008;28:1458–64.
28. Sun L, Liao K, Hang C, Wang D. Honokiol induces reactive oxygen species-mediated apoptosis in *Candida albicans* through mitochondrial dysfunction. PLoS ONE. 2017;12:e0172228.
29. Rauf A, Olatunde A, Imran M, Alhumaydhi FA, Aljohani ASM, Khan SA, et al. Honokiol: a review of its pharmacological potential and therapeutic insights. Phytomed Int J Phytother Phytopharmacol. 2021;90:153647.
30. Zhu J, Xu S, Gao W, Feng J, Zhao G. Honokiol induces endoplasmic reticulum stress-mediated apoptosis in human lung cancer cells. Life Sci. 2019;221:204–11.
31. Zhong ZH, Guo WL, Lei Y, Wang F, Wang SF, Sun Y, et al. Antiparasitic efficacy of honokiol against *Cryptocaryon irritans* in Pompano, *Trachinotus ovatus*. Aquaculture. 2019;500:398–406.
32. Zhang L, Dong L, Yang L, Luo Y, Chen F. MiR-27a-5p regulates acrylamide-induced mitochondrial dysfunction and intrinsic apoptosis *via* targeting *Btf3* in Rats. Food Chem. 2022;368:130816.
33. Li Z, Li X, Liu T, Chen S, Liu H, Wang H, et al. The critical roles of exposed surface residues for the thermostability and halotolerance of a novel GH11 xylanase from the metagenomic library of a saline-alkaline soil. Int J Biol Macromol. 2019;133:316–23.
34. Bai Y, Zhou Z, Zhao J, Ke Q, Pu F, Wu L, et al. The draft genome of *Cryptocaryon irritans* provides preliminary insights on the phylogeny of ciliates. Front Genet. 2022;12:808366.
35. Kroemer G, Galluzzi L, Vandenabeele P, Abrams J, Alnemri ES, Baehrecke EH, et al. Classification of Cell Death: recommendations of the nomenclature committee on cell death 2009. Cell Death Differ. 2009;16:3–11.
36. Dolai S, Adak S. Endoplasmic reticulum stress responses in *Leishmania*. Mol Biochem Parasitol. 2014;197:1–8.
37. Yeh PS, Wang W, Chang YA, Lin CJ, Wang JJ, Chen RM. Honokiol induces autophagy of neuroblastoma cells through activating the PI3K/Akt/mTOR and endoplasmic reticular stress/ERK1/2 signaling pathways and suppressing cell migration. Cancer Lett. 2016;370:66–77.
38. Chen YJ, Wu CL, Liu JF, Fong YC, Hsu SF, Li TM, et al. Honokiol induces cell apoptosis in human chondrosarcoma cells through mitochondrial dysfunction and endoplasmic reticulum stress. Cancer Lett. 2010;291:20–30.
39. Dolai S, Pal S, Yadav RK, Adak S. Endoplasmic reticulum stress-induced apoptosis in *Leishmania* through Ca^{2+}-dependent and caspase-independent mechanism. J Biol Chem. 2011;286:13638–46.
40. Oakes SA, Papa FR. The role of endoplasmic reticulum stress in human pathology. Annu Rev Pathol. 2015;10:173–94.
41. Chiu CS, Tsai CH, Hsieh MS, Tsai SC, Jan YJ, Lin WY, et al. Exploiting honokiol-induced ER Stress CHOP activation inhibits the growth and metastasis of melanoma by suppressing the mitf and β-catenin pathways. Cancer Lett. 2019;442:113–25.
42. Liu SH, Lee WJ, Lai DW, Wu SM, Liu CY, Tien HR, et al. Honokiol Confers immunogenicity by dictating calreticulin exposure, activating ER stress and inhibiting epithelial-to-mesenchymal transition. Mol Oncol. 2015;9:834–49.
43. Breckenridge DG, Germain M, Mathai JP, Nguyen M, Shore GC. Regulation of apoptosis by endoplasmic reticulum pathways. Oncogene. 2003;22:8608–18.
44. Marchi S, Patergnani S, Missiroli S, Morciano G, Rimessi A, Wieckowski MR, et al. Mitochondrial and endoplasmic reticulum calcium homeostasis and cell death. Cell Calcium. 2018;69:62–72.
45. Burton GJ, Yung HW, Murray AJ. Mitochondrial—endoplasmic reticulum interactions in the trophoblast: stress and senescence. Placenta. 2017;52:146–55.
46. Bastida-Ruiz D, Aguilar E, Ditisheim A, Yart L, Cohen M. Endoplasmic reticulum stress responses in placentation—a true balancing act. Placenta. 2017;57:163–9.
47. Liu KS, Peng ZH, Cheng WJ, Dai CF, Tong H. Endoplasmic reticulum stress-induced apoptosis in the development of reproduction. Reproduct Contraception. 2016;27:51–9.
48. Cho JH, Jeon YJ, Park SM, Shin JC, Lee TH, Jung S, et al. Multifunctional effects of honokiol as an anti-inflammatory and anti-cancer drug in human oral squamous cancer cells and xenograft. Biomaterials. 2015;53:274–84.
49. Higo T, Hattori M, Nakamura T, Natsume T, Michikawa T, Mikoshiba K. Subtype-specific and ER lumenal environment-dependent regulation of inositol 1,4,5-trisphosphate receptor Type 1 by ERp44. Cell. 2005;120:85–98.
50. Hara T, Mahadevan J, Kanekura K, Hara M, Lu S, Urano F. Calcium efflux from the endoplasmic reticulum leads to β-cell death. Endocrinology. 2014;155:758–68.
51. Kopil CM, Siebert AP, Foskett JK, Neumar RW. Calpain-cleaved Type 1 Inositol 1,4,5-trisphosphate receptor Impairs ER Ca^{2+} buffering and causes neurodegeneration in primary cortical neurons. J Neurochem. 2012;123:147–58.
52. Fan TJ, Han LH, Cong RS, Liang J. Caspase family proteases and apoptosis. Acta Biochim Biophys Sin. 2005;37:719–27.
53. Dixit R, Tiwari R, Katyal A, Pandey KC. Metacaspases: potential drug target against protozoan parasites. Front Pharmacol. 2019;10:790.
54. Huh SU. Evolutionary diversity and function of metacaspases in plants: similar to but not caspases. Int J Mol Sci. 2022;23:4588.
55. Murphy MP. How mitochondria produce reactive oxygen species. Biochem J. 2009;417:1–13.
56. Görlach A, Klappa P, Kietzmann T. The endoplasmic reticulum: folding, calcium homeostasis, signaling, and redox control. Antioxid Redox Signal. 2006;8:1391–418.
57. Estaquier J, Vallette F, Vayssiere JL, Mignotte B. The mitochondrial pathways of apoptosis. Adv Exp Med Biol. 2012;942:157–83.
58. Mashima T, Naito M, Tsuruo T. Caspase-mediated cleavage of cytoskeletal actin plays a positive role in the process of morphological apoptosis. Oncogene. 1999;18:2423–30.
59. Amé JC, Spenlehauer C, de Murcia G. The PARP superfamily. BioEssays. 2004;26:882–93.
60. Gourlay CW, Ayscough KR. The actin cytoskeleton in ageing and apoptosis. FEMS Yeast Res. 2005;5:1193–8.
61. Zhu M, Yang T, Wei S, DeWan AT, Morell RJ, Elfenbein JL, et al. Mutations in the gamma-actin gene (*ACTG1*) are associated with dominant progressive deafness (DFNA20/26). Am J Hum Genet. 2003;73:1082–91.
62. Erba HP, Eddy R, Shows T, Kedes L, Gunning P. Structure, chromosome location, and expression of the human gamma-actin gene: differential evolution, location, and expression of the cytoskeletal beta- and gamma-actin genes. Mol Cell Biol. 1988;8:1775–89.
63. Drazic A, Aksnes H, Marie M, Boczkowska M, Varland S, Timmerman E, et al. NAA80 is Actin's N-terminal acetyltransferase and regulates cytoskeleton assembly and cell motility. Proc Natl Acad Sci USA. 2018;115:4399–404.
64. Chen Q, Kassab MA, Dantzer F, Yu X. PARP2 Mediates Branched Poly ADP-ribosylation in Response to DNA Damage. Nat Commun. 2018;9:3233.
65. Bilokapic S, Suskiewicz MJ, Ahel I, Halic M. Bridging of DNA breaks activates PARP2-HPF1 to modify chromatin. Nature. 2020;585:609–13.
66. Obaji E, Maksimainen MM, Galera-Prat A, Lehtiö L. Activation of PARP2/ARTD2 by DNA damage induces conformational changes relieving enzyme autoinhibition. Nat Commun. 2021;12:3479.
67. Elmore S. Apoptosis: a review of programmed cell death. Toxicol Pathol. 2007;35:495–516.

68. Majtnerová P, Roušar T. An overview of apoptosis assays detecting DNA fragmentation. Mol Biol Rep. 2018;45:1469–78.
69. D'Arcy MS. Cell death: a review of the major forms of apoptosis necrosis and autophagy. Cell Biol Int. 2019;43:582–92.
70. Untergasser A, Cutcutache I, Koressaar T, Ye J, Faircloth BC, Remm M, et al. Primer3–new capabilities and interfaces. Nucleic Acids Res. 2012;40:e115.

Publisher's Note